Available online at www.sciencedirect.com
ScienceDirect
Journal of Sound and Vibration 321 (2009) 605–619
JOURNAL OF SOUND AND VIBRATION
www.elsevier.com/locate/jsvi

Acoustic imaging using under-determined inverse approaches: Frequency limitations and optimal regularization

Q. Leclère*

Laboratoire Vibrations Acoustique, INSA Lyon, 25 bis avenue Jean Capelle, F-69621 Villeurbanne Cedex, France

Received 16 July 2008; received in revised form 16 October 2008; accepted 22 October 2008
Handling Editor: C.L. Morfey
Available online 6 December 2008

Abstract

This paper presents an acoustic imaging technique based on an under-determined inverse approach. The principle is to quantify an elementary source distribution on a source surface from acoustic pressure measurements. The acoustic transfer system between elementary sources and microphone positions, very under-determined, is then reduced to a square system using singular value decomposition. The high frequency limitation of this method is studied, as well as the regularization techniques that have to be used at low frequency. A Monte-Carlo simulation is carried out to compare the efficiency of generalized cross validation and L-curve validation to choose the Tikhonov regularization parameter. A combined validation criterion is finally proposed to take advantage of both approaches.

1. Introduction

Acoustic imaging technologies have seen constant development over the past decades. Two main approaches must be distinguished: the beamforming technique, first introduced by Billingsley and Kinns [1], and the nearfield acoustical holography (NAH) technique [2]. The basic principle of beamforming is processing microphone signals with adequate time delays in order to obtain constructive interferences for acoustic waves coming from one particular direction. The main advantage of beamforming is the robustness of the method, while the drawbacks are its resolution limitations at low frequency, and its qualitative-only assessment of acoustic source strengths. NAH, contrary to beamforming, is based on acoustic measurements in the nearfield of the studied source. This method, more sophisticated than beamforming, is based on a numerical treatment of the acoustic pressures recorded by microphones, allowing one to 'retro-propagate' the acoustic waves from the measurement surface to the source surface. Initially based on DFT (discrete Fourier transform) algorithms [2,3], the NAH was subject to limitations such as the forced 2D periodicity of the sound field, requiring the use of spatial windowing, or the geometry of the problem, restricting the retro-propagation to geometrically simple sources (planar, spherical or cylindrical sources, see Ref. [4]). The method has been extended to identification procedures using a matrix formulation of the acoustic radiation [5]. The acoustic

*Fax: +33 472 438 712.
E-mail address: quentin.leclere@insa-lyon.fr

0022-460X/$ - see front matter © 2007 Elsevier Ltd. All rights reserved.
doi:10.1016/j.jsv.2008.10.022

Nomenclature

$\mathbf{h}$	$(m \times m)$ matrix of principal acoustic transfer functions
$\mathbf{h}_\beta$	regularized $(m \times m)$ matrix of principal acoustic transfer functions
$\mathbf{H}$	$(m \times n)$ matrix of acoustic transfer functions
$\mathbf{I}_{(s\times s)}$	$(s \times s)$ identity matrix
m	number of microphones
n	number of monopoles
$\mathbf{p}$	$(m \times 1)$ vector of acoustic pressures at a given frequency
$\mathbf{q}$	$(n \times 1)$ vector of monopole volumetric velocities
$\mathbf{Q}$	$(m \times 1)$ vector of principal sources
$\mathbf{Q}_\beta$	regularized $(m \times 1)$ vector of principal sources
r_β	residue of the regularized inverse problem
β	Tikhonov regularization parameter
ε	(simulation result) normalized error
ζ	condition number threshold for the CbV
η_β	$\log(\|\mathbf{Q}_\beta\|)$
ρ_β	$\log(r_\beta)$
τ	(simulation result) tendency of a method to over or under regularize
CbV	combined validation
DFT	discrete Fourier transform
dof	degree of freedom
GCV	generalized cross validation
(I)BEM	(inverse) boundary element method
(I)FRF	(inverse) frequency response function
LCV	L-curve validation
MSE	min square error
NAH	nearfield acoustical holography
NR	non-regularized
SNR	signal to noise ratio
(T)SVD	(truncated) singular value decomposition

radiation is computed using either a simple Green function (monopoles or dipoles) [6,7], spherical harmonics expansions [8], spherical wave-functions [9] or using boundary element formulations [5,10]. The superiority of matrix-based methods over DFT-based methods is highlighted in Ref. [11], their only drawback being a heavier computation time.

The advantages of such techniques compared to beamforming are an enhanced resolution at low frequency, and the quantitative assessment of source strengths. The major drawback is a heavier computation time (at least for matrix-based methods), and the sensitivity inherent to identification problems inducing the necessity to finely regularize the inversion step, either for DFT-based methods (filtering process in the k-space) or for matrix-based methods (filtering using singular value decomposition, SVD), which are still under investigation [12–16].

The aim of this paper is to describe the extension of inverse frequency response function (IFRF) methods to under-determined source–receiver systems. In classical IFRF applications, the number of sources mapping the radiating object has to be less than or equal to the number of microphone positions [7,15,17–19]. This can be problematic when a limited number of microphones is used, because source surfaces are too poorly discretized, and geometrical mismatches between discrete monopoles used to build the transfer system and real sources can induce high bias error [20]. The idea developed in this paper is to formulate the inverse system with a number of sources much greater than the number of microphones, and then to reduce source degrees of freedom (dofs) using a SVD approach. The idea to solve such an under-determined system is not new and is currently used in inverse BEM. Indeed, using BEM methods for inverse acoustic problems requires a fine discretization of the source geometry, and the number of source dofs—normal velocities at nodes—can be excessively large. This difficulty can be alleviated by using a base of wave-envelope vectors [21], or by applying SVD to acoustic transfer matrices resulting from direct BEM computations [22,23]. This paper proposes using a similar approach to inverse acoustic formulations using monopole distributions. The aim of this work is to highlight high frequency limitations and to determine an appropriate regularization procedure. The basics of IFRF-based acoustic imaging techniques are reviewed in the first part of this paper, with the proposed extension to under-determined IFRF systems. The second part of the work deals with the high frequency limitations of the approach. The third part is dedicated to the application of two well-known regularization methods for adjusting the Tikhonov regularization parameter: the generalized cross validation and the

L-curve. Both methods are compared within the framework of a Monte-Carlo simulation leading to the suggestion of a combined validation (CbV) procedure taking advantages of both techniques.

2. The IFRF method for acoustic source identification

2.1. The classic over-determined case

The inverse FRF theory is well developed in the work by Nelson and Yoon [13,17]. However, the general formulation will be briefly reviewed as an introduction to further developments.

The acoustic pressure hologram measured by the microphone array is represented by a complex vector $\mathbf{p}$ (size m × 1) depending on the frequency. Some pre-processing tools have to be applied if the microphone signals are not fully coherent, resulting in the decomposition of the measured sound field in several pressure holograms [24,25]. An acoustic transfer function matrix is built between the acoustic pressure at microphone positions and some source dofs. This transfer matrix can be measured (see Ref. [26]), but is more often computed using either boundary elements [18,21,27,28] or more simply using the monopole's Green function [7,17]. In the latter case, source dofs are the volumetric velocities of the monopoles noted $\mathbf{q}$ (size $n \times 1$):

$$\mathbf{p} = \mathbf{H}\mathbf{q} \tag{1}$$

with $\mathbf{H}$ the $m \times n$ matrix of acoustic transfer functions. Each element of the transfer matrix is computed using the monopole radiation formula

$$H = \mathrm{j}\rho\omega \frac{\mathrm{e}^{-\mathrm{j}kr}}{4\pi r} \tag{2}$$

with r the distance between the considered source–receiver couple (in m), k the acoustic wavenumber (in rad/m), ω the pulsation (in rad/s), and ρ the density of the fluid (in kg/m^3).

Generally, it is assumed that the number n of source dofs has to be less than or equal to the number m of microphones, as stated in Refs. [7,15,17–19]. The computation of $\mathbf{q}$ from $\mathbf{p}$ and $\mathbf{H}$ requires a matrix inversion. The difficulty is that this inversion is often ill-conditioned. In such cases, the classic left pseudo-inverse expressed by $\mathbf{H}^{+L} = (\mathbf{H}^*\mathbf{H})^{-1}\mathbf{H}^*$ (with subscript * for the Hermitian transpose) does not yield satisfying results, and a regularization procedure has to be implemented. Two techniques are currently used to regularize the inversion, namely Tikhonov and TSVD; they can both be expressed using the SVD of matrix $\mathbf{H}$

$$\mathbf{H}_{(m\times n)} = \mathbf{U}_{(m\times n)}\mathbf{S}_{(n\times n)}\mathbf{V}^*_{(n\times n)} \tag{3}$$

with * for the Hermitian transpose, $\mathbf{S}_{(n\times n)}$ the diagonal matrix of singular values sorted in decreasing order, $\mathbf{V}_{(n\times n)}$ a unitary matrix and $\mathbf{U}_{(m\times n)}$ truncated unitary matrix such that $\mathbf{U}^*_{(n\times m)}\mathbf{U}_{(m\times n)} = \mathbf{I}_{(n\times n)}$.

The inversion of matrix $\mathbf{H}$ from Eq. (3) is easily calculated due to the properties of the decomposition matrices. The ill-conditioned nature of the inversion comes from the very small singular values that are over-amplified by the inversion process. A first regularization method, named TSVD (for truncated SVD), consists in the suppression of these unstable components. A second approach, the Tikhonov regularization, consists in the amplification of the smallest singular values to decrease their magnitude once they are inverted.

The TSVD solution is given by

$$\mathbf{q} = \mathbf{V}_{(n\times r)}\mathbf{S}^{-1}_{(r\times r)}\mathbf{U}^*_{(r\times m)}\mathbf{p} \tag{4}$$

with $\mathbf{V}_{(n\times r)}$ the r firsts left columns of $\mathbf{V}_{(n\times n)}$, $\mathbf{U}_{(m\times r)}$ the r firsts left columns of $\mathbf{U}_{(m\times n)}$, and $\mathbf{S}_{(r\times r)}$ diagonal matrix of the r greatest singular values.

The Tikhonov solution is written as follows:

$$\mathbf{q} = \mathbf{V}_{(n\times n)}(\mathbf{S}_{(n\times n)} + \beta^2\mathbf{S}^{-1}_{(n\times n)})^{-1}\mathbf{U}^*_{(n\times m)}\mathbf{p} \tag{5}$$

with β a real positive regularizing parameter.

Both methods result in filters attenuating the effects of the smallest singular values. The difference is that the TSVD filter has an infinite cut-off slope, while Tikonov's has a slope adjusted on the singular values strengths.

The principal difficulty of regularization is the adjustment of a parameter, either r (integer between 1 and n) for TSVD or β (positive real number) for Tikhonov. The parameters r and β describe a singular value low pass filter, continuous for Tikhonov and discrete for TSVD. Several approaches are available to set the parameter value, the most popular ones being the Morozov discrepancy principle, based on an a priori knowledge of the error amount, ordinary and generalized cross validation (OCV and GCV) (see Refs. [12,13,29]) and the L-curve method [18,30]. A detailed overview of the numerical aspects of these methods is given in Ref. [31].

2.2. The under-determined case

The major limitation of IFRF techniques for imaging applications is that the number of sources is bounded by the number of microphones to ensure the uniqueness of the solution to the inverse problem. Consequently, the mapping of a source with a sufficient resolution requires a large number of microphones, resulting in a costly and difficult measurement process. We investigate in this work the possibility of taking into account a number of sources significantly greater than the number of microphones. This approach belongs to the class of under-determined problems, having an infinite number of solutions, which is why it is not implemented in classical IFRF methods. However, regularization techniques are currently used in IFRF applications, and a definition of regularization [32] is that a choice has to be made between several quasi-solutions. Thus, solving an IFRF system with regularization can consequently be considered as an under-determined problem. So we ask why should the number of source dofs always be bounded by the number of microphones?

As described in the previous section, applying regularization results in a low pass filtering of the effect of the singular values on the inverse solution. Several singular values can be rejected or strongly attenuated by this operation. Eq. (4) can be written as follows:

$$\mathbf{q} = \mathbf{V}_{(n\times r)}\mathbf{S}^{-1}_{(r\times r)}\mathbf{P}_{(r\times 1)} \quad \text{with } \mathbf{P}_{(r\times 1)} = \mathbf{U}^{*}_{(r\times m)}\mathbf{p}. \tag{6}$$

In Eq. (6), the measured hologram is projected on a base of r orthogonal holograms (columns of $\mathbf{U}_{(m\times r)}$). This expression of the TSVD regularized solution shows the under-determined nature of the system: a set of n elementary sources is reconstructed from a set of r acoustic pressure dofs, with $r<n$. The main idea developed in this paper is that the solution expressed by Eq. (6) could have been found with a number r of microphones only.

Following these considerations, an under-determined IFRF system using the SVD is expressed by

$$\mathbf{p} = \mathbf{H}\mathbf{q} = \mathbf{U}_{(m\times m)}\mathbf{S}_{(m\times m)}\mathbf{V}^{*}_{(m\times n)}\mathbf{q} \quad \text{with } n>m \tag{7}$$

with $\mathbf{U}_{(m\times m)}$ unitary matrix, $\mathbf{S}_{(m\times m)}$ diagonal matrix of singular values, and $\mathbf{V}_{(n\times m)}$ such that $\mathbf{V}^{*}_{(m\times n)}\mathbf{V}_{(n\times m)} = \mathbf{I}_{(m\times m)}$.

The inversion of Eq. (7) leads to computation of the so-called right pseudo-inverse $\mathbf{H}^{+R} = \mathbf{H}^{*}(\mathbf{H}\mathbf{H}^{*})^{-1}$ of matrix $\mathbf{H}$, which is the standard way to deal with under-determined cases in linear algebra. If the smallest singular values of Eq. (7) are negligible, it means that the microphone density on the array is sufficient: a larger number of microphones would have only generated more negligible singular values. The under determination of the system is in this case induced by the acoustic propagation from the source plane to the measurement plane, smoothing high frequency details of the source. If the system does not require any regularization (if all singular values are consistent), it means that a larger number of microphones would have generated additional consistent singular values. In this case, the inversion of Eq. (7) can lead to erroneous results, because Shannon's sampling criterion is possibly not satisfied on the measurement plane.

Principal sources are defined by the product $\mathbf{V}^{*}_{(m\times n)}\mathbf{q}$. Thus, Eq. (7) can be inverted

$$\mathbf{Q} = \mathbf{S}^{-1}_{(m\times m)}\mathbf{U}^{*}_{(m\times m)}\mathbf{p} \quad \text{with } \mathbf{Q} = \mathbf{V}^{*}_{(m\times n)}\mathbf{q} \text{ principal sources.} \tag{8}$$

Once principal sources are obtained, real sources $\mathbf{q}$ have to be assessed, and this is not straightforward because the product $\mathbf{V}_{(n\times m)}\mathbf{V}^{*}_{(m\times n)}$ is not an identity matrix. Meanwhile, a set of equivalent sources $\tilde{\mathbf{q}}$ can be expressed as follows:

$$\tilde{\mathbf{q}} = \mathbf{V}_{(n\times m)}\mathbf{Q}, \tag{9}$$

which corresponds to the minimum length solution of the under-determined system. The relation between real sources $\mathbf{q}$ and equivalent sources $\tilde{\mathbf{q}}$ is expressed by

$$\tilde{\mathbf{q}} = \mathbf{V}_{(n\times m)}\mathbf{V}^{*}_{(m\times n)}\mathbf{q}. \tag{10}$$

This relation is very important because it is an a priori indication of the bias induced by the approach between real and equivalent sources.

A computational example of equivalent sources is given for a rectangular microphone array ($6 \times 5 = 30$ microphones). The 644 elementary sources are distributed on a rectangular surface (56×46 cm), with a resolution of 2 cm. The distance between microphones is 10 cm, and the dimensions of the array are 50×40 cm. The array is located 20 cm from the source plane. The projection of each principal source on the source surface is given by each column of the $\mathbf{V}_{(n\times m)}$ matrix (see Eq. (9)). The projection of the nine first principal sources on equivalent ones is shown in Fig. 1 for 1000 Hz. The total number of principal sources is equal to the number of microphones, 30 in this case.

Equivalent sources are obtained by a linear combination of principal sources. A single monopole type source distribution and its equivalent sources computed with Eq. (10) are shown in Fig. 2 for several frequencies. For single monopole sources, equivalent sources correspond to columns of the $\mathbf{V}_{(n\times m)}\mathbf{V}^{*}_{(m\times n)}$ product. The position of the maximum of the equivalent sources coincides with the original one, which validates the operation. The diameter of the equivalent sources does not depend on the frequency below 2 kHz: the diameter is almost equal to the distance between microphones on the array. For frequencies higher than 2 kHz, the diameter of equivalent sources decreases, but we also note the appearance of significant 'ghost images' which illustrates the high frequency limitation of the method. At high frequencies, the number of significant singular values of system (8) is bounded by the number of microphones. In this case, sources can induce some details on the hologram plane that have larger spatial frequencies than the half spatial sampling of the array, i.e. Shannon's criterion is potentially no longer satisfied. The high frequency limitation of the method is studied in the following section.

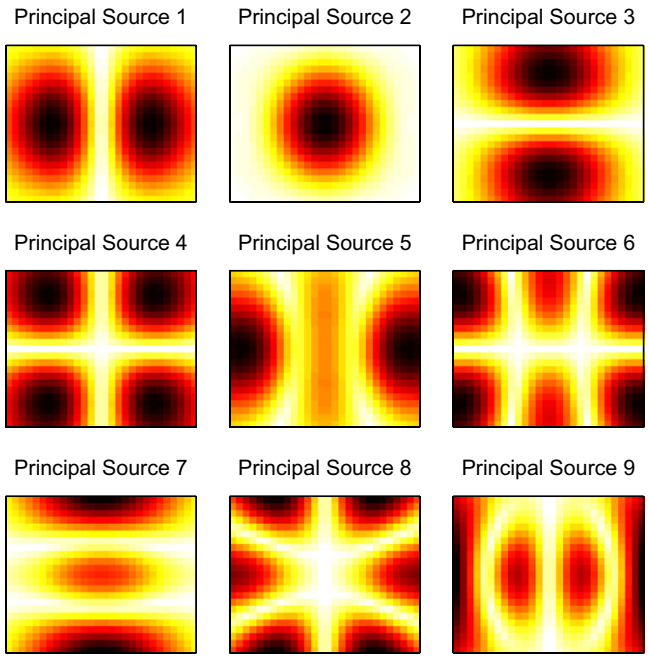

Fig. 1. Projection of the nine first principal sources (magnitude) on the source surface at 1 kHz. Color scale from white (zero) to black (max. value).

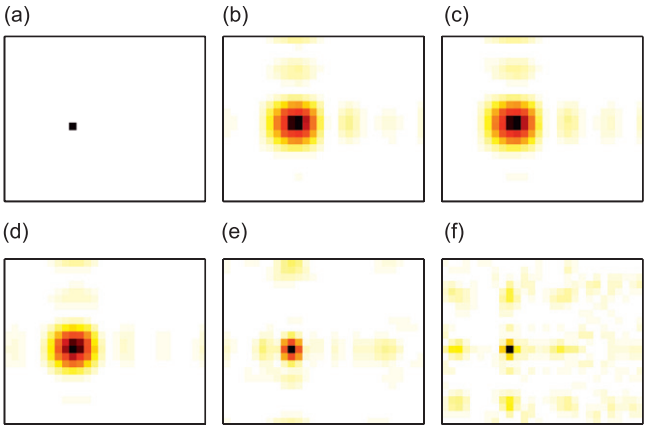

Fig. 2. Single monopole type source $\mathbf{q}$ (a), and equivalent sources $\tilde{\mathbf{q}}$ at 500 Hz (b), 1 kHz (c), 2 kHz (d), 4 kHz (e) and 6 kHz (f), linear scale. Color scale from white (zero) to black (max. value).

3. High frequency limitations of the under-determined IFRF method

It has been shown in the previous section that the under-determined IFRF method is valid if the number of significant singular values is less than the number of microphones. Thus, the condition number of the transfer matrix can be a good indicator to validate a result (the condition number is the ratio between the largest and the smallest singular value). At high frequencies, the smallest singular values are not negligible, equivalent sources are distorted by the appearance of ghost images. According to Eq. (10), columns of matrix $[V]_{nm}[V]^*_{mn}$ are equivalent sources corresponding to each monopole of the source surface. The appearance of ghost images can be assessed for single monopole sources, by computing the average distance between the real source and monopoles of the surface, weighted by their magnitudes

$$R_i = \frac{\sum_j |\tilde{q}_{ij}| r_{ij}}{\sum_j |\tilde{q}_{ij}|} \tag{11}$$

with R_i mean distance between the i monopole and its equivalent source, $|\tilde{q}_{ij}|$ jth row of the ith column of the product $\mathbf{V}_{(n\times m)}\mathbf{V}^*_{(m\times n)}$, and r_{ij} the distance between ith and jth monopoles.

The mean distance, R_i, is an indicator of the concentration of the equivalent source distribution representing the ith monopole.

The condition number of the transfer matrix is drawn as a function of the frequency in Fig. 3 (on the left) for the same numerical experiment as in the previous section. The mean distance averaged for all monopoles is also drawn in Fig. 3 (on the right), with for each frequency line the maximum and minimum values.

Below 3 kHz, the condition number of the transfer matrix decreases when the frequency increases. Above this frequency, the condition number is stable around 2, which means that the smallest singular value is equal to 50 percent of the greatest one. It can be said that the smallest singular value begins to be significant above 2 kHz (10 percent of the greatest one). We see on the right of Fig. 3 that the mean distance is relatively stable below 2 kHz around 14 cm. Between 2 and 3 kHz, we note an abrupt increase of the mean distance, which is the consequence of the appearance of ghost images. Above 3 kHz, the mean distance remains relatively stable around 23 cm. These observations show that the method is valuable below 2 kHz, and that erroneous results can be obtained above this frequency.

Fig. 3 shows that the mean distance R can be very different from one monopole to the other: the maximum curve is about two times the minimum one. A map of mean distance can be drawn for a given frequency, showing regions of the source surface that are particularly affected by ghost images. Such maps are shown in Fig. 4 at 2 and 4 kHz.

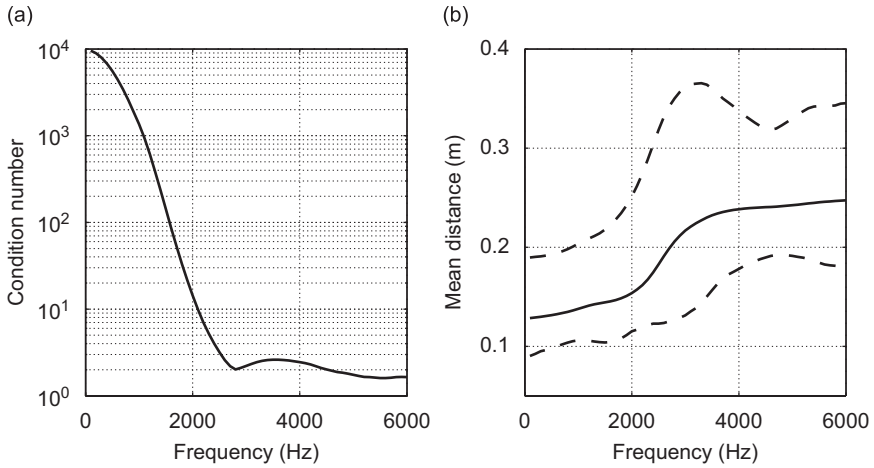

Fig. 3. (a) Condition number of the transfer matrix **H**. (b) — Averaged, - - - minimum and maximum values of the mean distance between monopoles and equivalent sources.

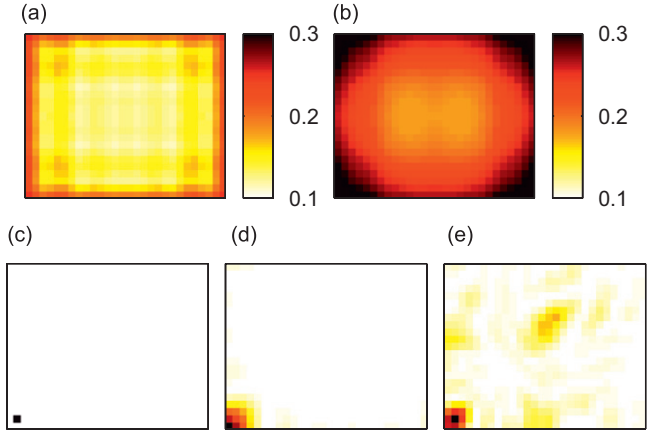

Fig. 4. Mean distance between monopoles and equivalent sources at: (a) 2 kHz, (b) 4 kHz. Edge monopole (c), equivalent sources at 2 kHz (d) and 4 kHz (e), linear scale.

The maps of mean distance show that the more distant the monopoles are from the center of the source plane, the more their equivalent sources are subject to the appearance of ghost images. At 2 kHz, the mean distance is important only on the edge of the monopole surface. At 4 kHz, the mean distance remains more important at the edge, but the region is much more pronounced and extended. An example of an edge monopole and its equivalent sources are shown in Fig. 4 (at the bottom). It is clear that ghost images are more significant at 4 kHz for a monopole at the edge than for a central monopole (see Fig. 2). This phenomenon can be explained by the position of the considered monopole relative to the microphone grid position. Indeed, the source surface has the same size as the microphone array. The solid angle covered by the microphone grid is thus much more important for a central monopole than for an edge monopole. The ability of the array to correctly identify sources is thus logically better at the center of the source plane.

A parallel can be drawn at this stage with beamforming approaches. In fact, the under-determined IFRF method and beamforming are both based on the same formulation of the acoustic radiation of a distribution of elementary sources; it is thus convenient to compare them in some application cases [33,35]. The major difference is that beamforming involves a term-by-term inversion of the **H** matrix, while inverse FRF involves a matrix inversion [20]. The consequence is that beamforming is a qualitative-only approach, contrary to the

method presented in this work. Another consequence is that the low frequency resolution of beamforming is limited compared to the proposed method. At high frequencies, both methods are affected by ghost images, however, some of our previous work shows that in similar cases [34,35], the inverse FRF method is less affected by ghost images than beamforming.

An important parameter affecting ghost images is the geometry of the array. It is well known, for beamforming applications, that the rectangular grid is not the best solution. Solutions using optimized array shapes (circular, random) are already available. It is likely that this types of geometrical configurations will improve the high frequency results presented in this section, but this is not the aim of the present work.

The under-determined IFRF approach is theoretically only limited at high frequencies. It has been shown in the previous section that the diameter of equivalent sources tends at low frequency towards the distance between microphones on the array. Meanwhile, we have also seen that the condition number of the transfer matrix is very high at low frequency (see Fig. 3), inducing a high sensitivity to the inversion process. At low frequency, regularization procedures have to be applied, decreasing the spatial resolution of the method. Regularization procedures are the subject of the following section.

4. Optimal regularization of the under-determined IFRF method

The direct problem linking acoustic pressures $\mathbf{p}$ to principal sources $\mathbf{Q}$ is written as follows:

$$\mathbf{p} = \mathbf{H}\mathbf{q} = \mathbf{U}_{(m\times m)}\mathbf{S}_{(m\times m)}\mathbf{V}^*_{(m\times n)}\mathbf{q} = \mathbf{h}\mathbf{Q} \tag{12}$$

with $\mathbf{h} = \mathbf{U}_{(m\times m)}\mathbf{S}_{(m\times m)}$ the principal acoustic transfer matrix between principal sources and microphone positions and $\mathbf{Q} = \mathbf{V}^*_{(m\times n)}\mathbf{q}$ principal source dofs.

Eq. (8) is a square system giving principal source strength as a function of measured acoustic pressures, it is thus equivalent to classical acoustic inverse problems, needing regularization if badly conditioned. The Tikhonov regularization is adjusted by varying β in the following equation:

$$\mathbf{Q}_\beta = (\mathbf{S}_{(m\times m)} + \beta^2\ \mathbf{S}^{-1}_{(m\times m)})^{-1}\mathbf{U}^*_{(m\times m)}\mathbf{p} = \mathbf{h}^{-1}_\beta\mathbf{p}. \tag{13}$$

The methods used to adjust β involve a quantity called the residue, equal to the distance between inputs of the inverse problem $\{p\}_m$ and outputs of the direct problem fed with the regularized solution

$$r_\beta = \|\mathbf{p} - \mathbf{h}\mathbf{Q}_\beta\| = \|(\mathbf{I}_{(m\times m)} - \mathbf{h}\mathbf{h}^{-1}_\beta)\mathbf{p}\|. \tag{14}$$

4.1. Adjusting the regularization parameter

Two methods will be compared and combined to adjust the regularization parameter: the GCV and the LCV. These methods, well described in Ref. [31], have the advantage that they do not require some presumed knowledge of the error level in the observations $\mathbf{p}$.

4.1.1. Generalized cross validation

GCV (generalized cross validation) [29] is a first approach for adjusting β. This approach is an extension of the OCV principle, a method based on the ability of the solution obtained with $(m-1)$ observations to predict the mth one. The GCV function, that has to be minimized, is given by

$$J_{\mathrm{GCV}}(\beta) = \frac{r^2_\beta}{\mathrm{Tr}(\mathbf{I}_{(m\times m)} - \mathbf{h}\mathbf{h}^{-1}_\beta)^2} \tag{15}$$

with $\mathrm{Tr}(\mathbf{X})$ for the trace of matrix $\mathbf{X}$.

The denominator of the GCV function is an estimation of the bias induced by β. Without any regularization ($\beta = 0$), this quantity is equal to zero, because $\mathbf{h}\mathbf{h}^{-1}_\beta$ is equal to $\mathbf{I}_{(m\times m)}$. When the amount of regularization

increases, the $\mathbf{hh}_{\beta}^{-1}$ matrix deviates from the identity matrix, increasing the value of the denominator of $J_{\mathrm{GCV}}(\beta)$.

4.1.2. The L-curve validation

The L-curve is the name given to the parametric curve representing the logarithm of the norm of the solution $\|\mathbf{Q}\|$ as a function of the logarithm of the residue r, for different values of the regularizing parameter β [30]. With little regularization, the norm of the regularized solution decreases sharply with β with little change in the residual norm: this is the 'vertical' part of the L-curve. With too much regularization, the residual norm significantly increases with β while the norm of the regularized solution only slightly decreases: this is the horizontal part of the L-curve. The best value for β stands at the corner of the L-curve: this is the best compromise between the minimization of $\|\mathbf{Q}\|$ and r. The curve is plotted in a log–log scale because both quantities are not directly comparable and a relative scale has to be used. The corner of the curve is found numerically by computing the curvature of the L-curve, which has a maximum value at its corner. The curvature function is given by

$$J_{\mathrm{LCV}}(\beta)=\frac{\rho'_{\beta}\eta''_{\beta}-\rho''_{\beta}\eta'_{\beta}}{(\rho'^{2}_{\beta}+\eta'^{2}_{\beta},)^{3/2}} \quad \text{with } \rho_{\beta}=\log(r_{\beta}),$$

$$\eta_{\beta}=\log(\|\mathbf{Q}_{\beta}\|), \tag{16}$$

and $'$ and $''$, respectively, for first and second derivatives with respect to β.

The optimal value β_{LCV} corresponds to the curve's corner maximizing function $J_{\mathrm{LCV}}(\beta)$.

4.2. Monte-Carlo simulations to compare regularization methods

A numerical experiment is implemented to assess the ability of GCV and LCV to properly adjust β. The advantage of numerical experiments in comparing regularization methods is obviously that the 'exact' solution is available. Several papers from ISVR [15,36] compare LCV and GCV to adjust the Tikhonov regularization amount in the framework of numerical simulations, for, respectively, acoustic and vibration inverse problems. To compare solutions provided by LCV and GCV, they introduce a third validation criterion based on the knowledge of the exact solution. This indicator is obviously not available for experimental applications, but it allows one to compare objectively LCV and GCV solutions. This indicator, noted MSE for 'min square error' is given by

$$J_{\mathrm{MSE}}(\beta)=\|\mathbf{Q}_{\beta}-\mathbf{Q}_{\mathrm{exact}}\|, \tag{17}$$

the optimal value for β_{MSE} corresponding to the value of β minimizing the function $J_{\mathrm{MSE}}(\beta)$. The difference with paper [15] is that the so-called 'exact' solution does not correspond to the exact solution introduced in the direct problem $\mathbf{q}_{\mathrm{exact}}$ but to its corresponding principal source $\mathbf{Q}_{\mathrm{exact}}=\mathbf{V}^{*}_{(m\times n)}\mathbf{q}_{\mathrm{exact}}$. The performance of GCV and LCV can be assessed by computing Euclidean distances between GCV and LCV solutions and the MSE solution

$$\begin{cases}\varepsilon_{\mathrm{LCV}}=\dfrac{\|Q_{\mathrm{LCV}}-Q_{\mathrm{MSE}}\|}{\|Q_{\mathrm{MSE}}\|},\\ \varepsilon_{\mathrm{GCV}}=\dfrac{\|Q_{\mathrm{GCV}}-Q_{\mathrm{MSE}}\|}{\|Q_{\mathrm{MSE}}\|},\\ \varepsilon_{\mathrm{NR}}=\dfrac{\|Q_{\mathrm{NR}}-Q_{\mathrm{MSE}}\|}{\|Q_{\mathrm{MSE}}\|},\end{cases} \tag{18}$$

the 'best' regularization between $\mathbf{Q}_{\mathrm{LCV}}$ and $\mathbf{Q}_{\mathrm{GCV}}$ being provided by the solution minimizing its distance to the MSE solution $\mathbf{Q}_{\mathrm{MSE}}$. A third criterion $\varepsilon_{\mathrm{NR}}$ is computed corresponding to $\mathbf{Q}_{\mathrm{NR}}$, solution of the non-regularized inversion ($\beta_{\mathrm{NR}}=0$).

Moreover, comparing β_{GCV} and β_{LCV} to β_{MSE} leads to a determination if solutions are too much or not enough regularized

$$\begin{cases} \tau_{LCV} = \mathrm{sgn}(\beta_{LCV} - \beta_{MSE}), \\ \tau_{GCV} = \mathrm{sgn}(\beta_{GCV} - \beta_{MSE}), \\ \tau_{NR} = \mathrm{sgn}(-\beta_{MSE}) \end{cases} \tag{19}$$

with function $\mathrm{sgn}(x)$ giving 1 if $x>0$, 0 if $x=0$ and -1 if $x<0$.

If τ is equal to one (resp. minus one), the solution is not enough (resp. too much) regularized. Averaging this quantity over a large number of cases allows us to say if solutions are generally over-regularized (if $\langle\tau\rangle$ is close to one) or under-regularized (if $\langle\tau\rangle$ is close to minus one). If the average value $\langle\tau\rangle$ is close to zero, it means that there is no general trend concerning the over or under regularization.

The combined analysis of average values of $\langle\tau\rangle$ and $\langle\varepsilon\rangle$ for GCV and LCV over a large number of cases allows us to quantify the performance of regularization approaches and to determine, when the performance is not satisfying, whether the regularizations are too strong or too weak.

4.2.1. Geometry of the problem

The geometry taken for the simulations is identical to the geometry used in Section 2.2. The studied array is a rectangular microphone array ($6 \times 5 = 30$ microphones) with a 10 cm distance between microphones (50×40 cm). On a rectangular surface of 56×46 cm 644 elementary sources are distributed, with a resolution of 2 cm. The array is placed at a distance d from the source plane.

4.2.2. Course of the simulation

The simulation is carried out for different frequencies, different noise levels and different distances between source and microphone planes. For a given frequency, a given noise level and a given source–array distance, the following Monte-Carlo procedure is followed:

- build the transfer matrix at a given frequency and compute its SVD,
- for $k = 1$ to N,
  - *begin loop*,
  - choose randomly three monopole positions on the source distribution,
  - assign them random complex strength,
  - compute the acoustic pressures: $\mathbf{p} = \mathbf{Hq}$,
  - add noise on the acoustic pressures $\widetilde{\mathbf{p}}$,
  - find β^k_{MSE}, β^k_{LCV} and β^k_{GCV},
  - compute ε^k_{LCV}, ε^k_{GCV}, τ^k_{LCV} and τ^k_{GCV},
  - *end of loop*,
- compute average values $\langle\varepsilon\rangle_k$, $\langle\tau\rangle_k$ over k for GCV and LCV.

The noisy pressures $\widetilde{\mathbf{p}}$ are computed using multiplicative and additive perturbations, given for the ith microphone by

$$\widetilde{p_i} = p_i + 10^{SNR/20}\left(\alpha e^{j\theta} p_i + \delta e^{j\varphi}\sqrt{\frac{\|\mathbf{p}\|^2}{m}}\right) \tag{20}$$

with α and δ two zero-mean Gaussian random variables with $Var(\alpha) = Var(\delta) = 1$, and θ and φ two random variables uniformly distributed between 0 and 2π.

Simulations are carried out over 500 cases ($N = 500$), for SNR varying between 40 dB (1 percent noise) and 6 dB (50 percent noise) and from 100 to 2500 Hz. The results presented in the following have thus been obtained from about $1e6$ cases for each source–array distance d.

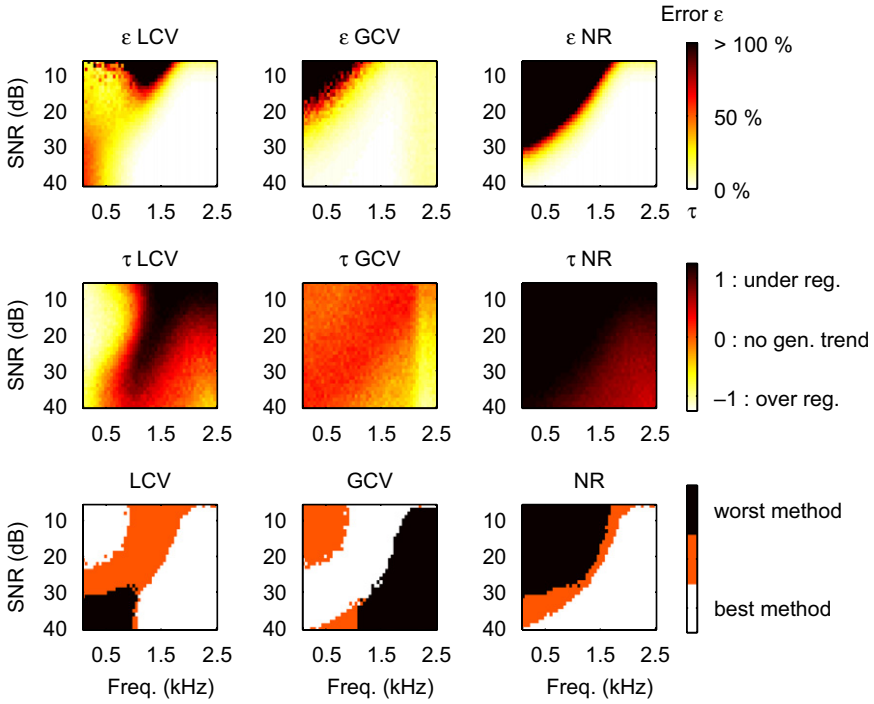

Fig. 5. Simulation results. Source–array distance = 10 cm. ε maps on the first row give the average error between the result given by LCV, GCV or NR and the optimal result MSE. τ maps on the second row indicate the tendency of LCV, GCV or NR to either over or underestimate the regularization amount. The maps at the third row of the figure only give the rank of the method given by the ε maps: the best method is the one with the lowest average error, and the worst is the one with the highest average error.

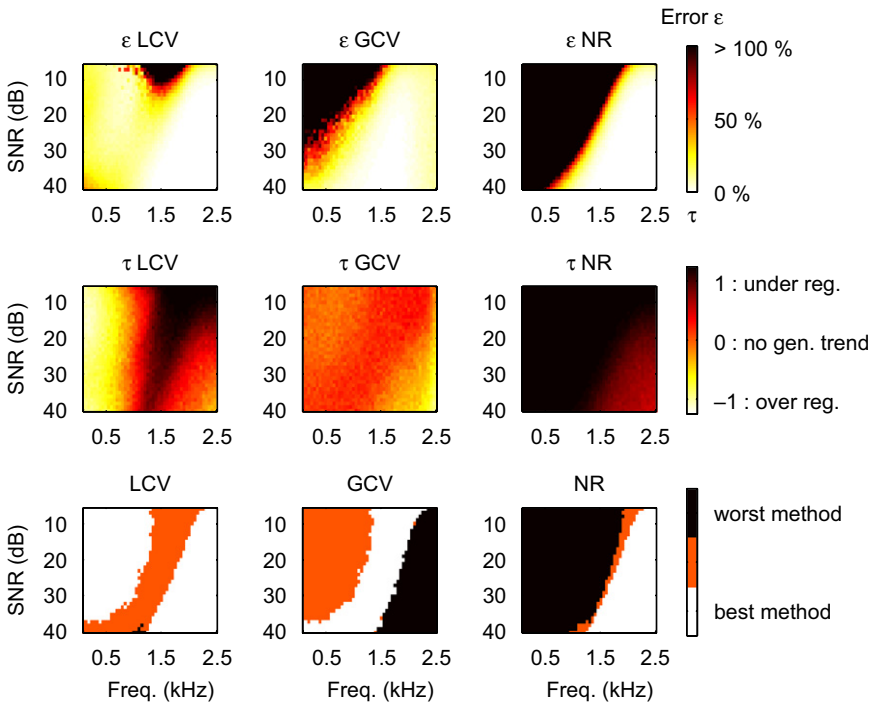

Fig. 6. Simulation results. Source–array distance = 15 cm.

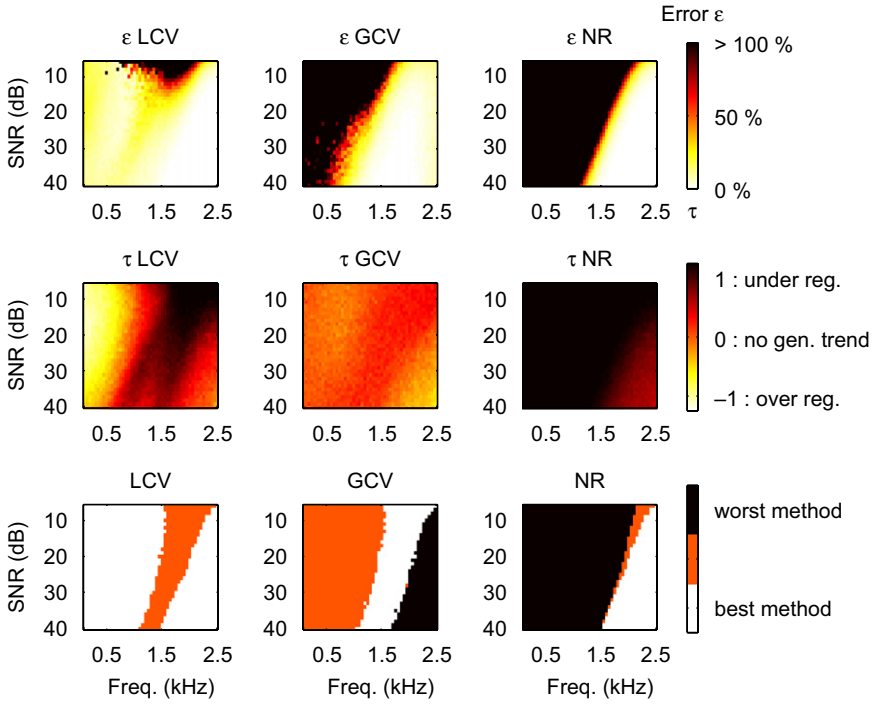

Fig. 7. Simulation results. Source–array distance = 20 cm.

4.2.3. Results of simulations

The results of the simulations are shown in Fig. 5 for a source–array distance $d = 10$ cm, in Fig. 6 for $d = 15$ cm and in Fig. 7 for $d = 20$ cm.

The LCV seems to give very satisfying results for all distances (low error function ε) except in a mid-frequency range (0.600–1.6 kHz at 10 cm, 1–2 kHz at 15 cm and 1.2–2.2 kHz at 20 cm) for low SNR values (<15 dB). The examination of the corresponding τ function allows one to say that the regularization amount according LCV is too weak in these frequency bands. The ε value for low frequency (<500 Hz) at 10 cm is also important because of a too strong regularization. Generally, for each distance, the LCV solution can be said to be over-regularized at low frequency, and under-regularized in a frequency band depending on both the source–array distance and on the SNR level. The good results obtained at high frequencies (low ε function) show that the LCV is also able to treat well-conditioned problems. In fact, when the L-curve's curvature is always negative (the concave case), it means that there is no corner. In this case, the LCV algorithm that was used applies no regularization. The mid-frequency range for which LCV generally under-regularizes the problem corresponds to conditions for which the corner of the curve is difficult to localize, or to situations for which the curve is concave, but for which a certain amount of regularization remains necessary to get the optimal MSE result.

The GCV is much more sensitive than the LCV to the source–array distance, i.e. to the conditioning of the problem. Indeed, the condition number increases dramatically with the source–array distance. The results obtained at 10 cm are quite satisfying, but results obtained at 15 and 20 cm are very disappointing at a wide low frequency range. Condition numbers of problems corresponding to different distances are drawn in Fig. 8. Concerning τ_{GCV}, averaged values are always around zero except at high frequencies, which means that there is no general trend about the tendency to over or underestimate the regularization amount. The high frequency error function ε_{GCV} is not bad, but it is the method providing the worst results, with a tendency to over-regularize the solution. Contrary to LCV, GCV is not able to treat the well-conditioned problem without regularization. It is interesting to note that results obtained using GCV are quite satisfying in a mid-frequency band in which the LCV is defective. GCV is indeed the method providing the best results in a mid-frequency band depending on both the SNR level and the source–array distance.

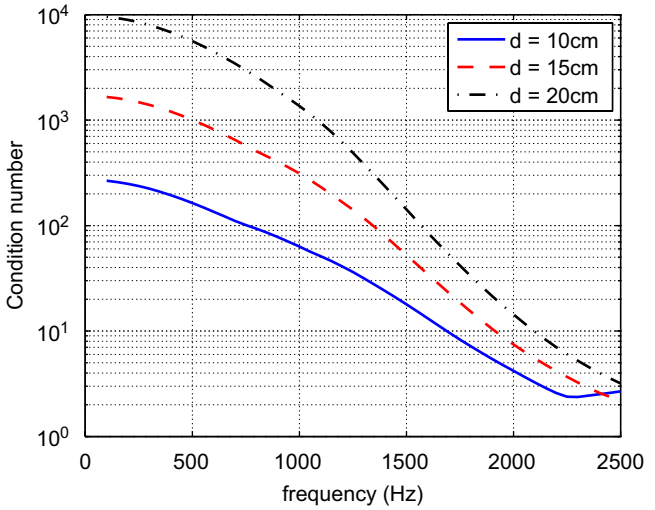

Fig. 8. Condition number of the **H** matrix as a function of the frequency for $d = 10, 15$ and 20 cm.

It can be seen that, for close distances (10 cm), low frequency, and high SNR, the best approach seems to be the non-regularized one. These levels of SNR (>30 dB) are in fact very difficult to obtain experimentally, if we include in the noise the uncertainty as to the global gain of the whole acquisition channels. It is experimentally known that for this kind of configuration of acoustic inverse problem and this frequency range (<500 Hz), a regularization is always necessary. Moreover, it would be hazardous to base the regularization amount on a hypothesis as to the SNR value (that is not a priori known). Finally, it can be seen, even if the best approach is the non-regularized one in this high SNR-low frequency area, that the error ε using LCV or GCV is not significantly greater than the error obtained without regularization.

4.3. Combining LCV and GCV to optimize the regularization

Results presented in the previous section show that LCV and GCV could be complementary. An indicator based on both GCV and LCV is proposed in order to find β_{CbV}. The idea is to keep the minimum β value provided by GCV and LCV. This CbV is supposed to give better results than GCV or LCV: at low frequency, the best method is the LCV, which generally regularizes more than the GCV ($\tau_{\mathrm{LCV}} < \tau_{\mathrm{GCV}}$). The CbV chooses the most important regularization amount; β_{CbV} will consequently be equal to β_{LCV} in this frequency range. In the mid-frequencies, in the area for which the LCV is defective, β_{LCV} is generally under-estimated, thus β_{CV} will be equal to β_{GCV}. A problem remains at high frequencies, when the inversion is well conditioned: the value of β_{CbV} will be provided by the GCV approach, applying a non-null regularization amount even for well-conditioned problems. A solution is to always keep the LCV solution for condition numbers lower than a given threshold ζ. The CbV indicator is thus expressed as follows:

$$\beta_{\mathrm{CbV}} = \begin{cases} \max(\beta_{\mathrm{LCV}}, \beta_{\mathrm{GCV}}) & \text{for cond } (\mathbf{H}) > \zeta, \\ \beta_{\mathrm{LCV}} & \text{for cond } (\mathbf{H}) < \zeta. \end{cases} \tag{21}$$

The results using this CbV, shown in Fig. 9 (threshold $\zeta = 10$), confirm these expectations. Error maps obtained with the CbV are very satisfying. The error function is relatively low and constant over the noise level-frequency map. The CbV seems to take advantages of both LCV and GCV. The maps at the bottom of Fig. 9 present a ranking of the four approaches (LCV, GCV, CbV and no regularization) given by the mean value of their ε function. The proposed CbV approach is the best one over a very wide frequency range, except for $d = 10$ cm at low frequency and high SNR values, an area for which the CbV is equal to the LCV, that over-regularizes the identification.

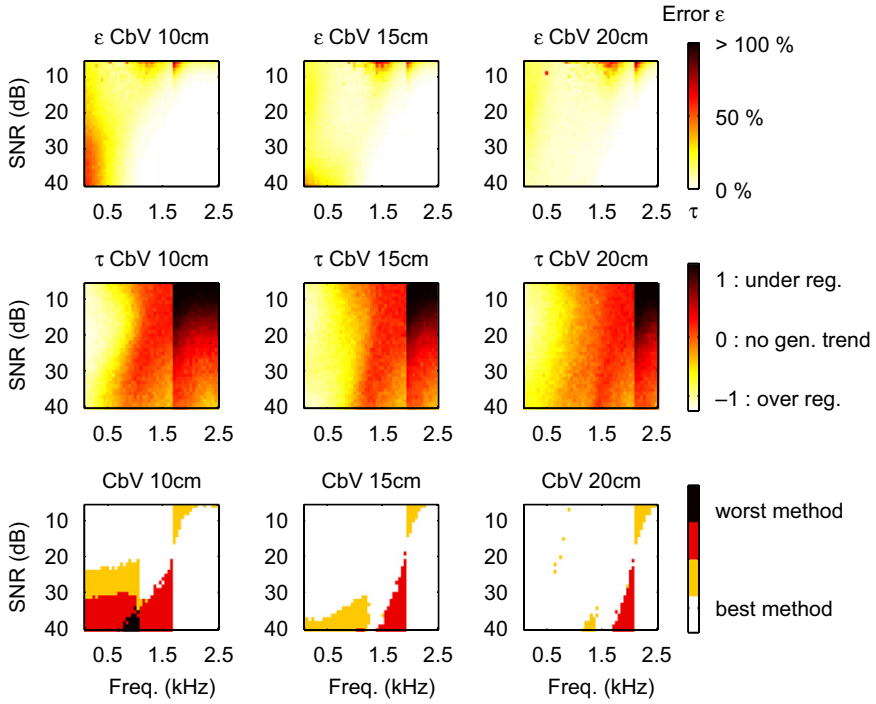

Fig. 9. Simulation results using the CbV indicator. Source–array distances = 10, 15, 20 cm. The maps at the third row of the figure just give the rank of the CbV method regarding ε compared to LCV, GCV and NR.

5. Conclusion

This paper proposes a method for acoustic imaging applications. The principle is to formulate the acoustic propagation between an elementary source distribution and a limited number of microphone positions. The inversion of this kind of transfer system is very under-determined: there are many more unknowns (elementary source strengths) than measured data (measured acoustic pressures). The number of source dofs is reduced using an SVD, allowing one to build a number of orthogonal source distributions equal to the number of microphones. This operation can be done without difficulty at low frequency, when the condition number of the transfer matrix is important. At high frequencies, this can lead to the appearance of ghost images, because of a lack of microphones. Two methods are tested in the framework of a Monte-Carlo simulation to regularize the inversion at low frequency: the generalized cross validation and the L-curve validation. Both methods are found to be complementary, and a mixed indicator is finally proposed that takes advantage of both methods. The efficiency of the combined validation is shown with the Monte-Carlo simulation for different source–array distances.

References

[1] J. Billingsley, R. Kinns, The acoustic telescope, *Journal of Sound and Vibration* 48 (4) (1976).
[2] E.G. Williams, J.D. Maynard, E. Skudrzyk, Sound source reconstructions using a microphone array, *Journal of the Acoustical Society of America* 68 (4) (1980) 340–344.
[3] J.D. Maynard, E.G. Williams, Y. Lee, Nearfield acoustic holography: I. Theory of generalized holography and the development of NAH, *Journal of the Acoustical Society of America* 78 (4) (1985) 1395–1413.
[4] E.G. Williams, *Fourier Acoustics*, Academic Press, New York, 1999.
[5] W.A. Veronesi, J.D. Maynard, Digital holographic reconstruction of sources with arbitrarily shaped surfaces, *Journal of the Acoustical Society of America* 85 (2) (1989) 588–598.

[6] G.H. Koopmann, L. Song, J.B. Fahnline, A method for computing acoustic fields based on the principle of wave superposition, *Journal of the Acoustical Society of America* 86 (6) (1989).
[7] S.M. Dumbacher, D.L. Brown, Source imaging of irregularly shaped surfaces using inverse FRF method, *Proceedings of ISMA 21*, Leuven, Belgium, 1996.
[8] F. Fazi, V. Brunel, P.A. Nelson, Spherical harmonic analysis applied to the reconstruction of the sound field radiated by a loudspeaker, *Proceedings of Acoustics 08*, Paris, France, 2008.
[9] S.F. Wu, X. Zhao, Combined Helmholtz equation: least squares method for reconstructing acoustic radiation from arbitrarily shaped objects, *Journal of the Acoustical Society of America* 112 (1) (2002) 179–188.
[10] M.R. Bai, Application of bem based acoustic holography to radiation analysis of sound sources with arbitrarily shaped surfaces, *Journal of the Acoustical Society of America* 92 (1) (1992).
[11] E.G. Williams, Comparison of svd and dft approaches for nah, *Proceedings of Inter-Noise 2002*, Dearborn, MI, USA, 2002.
[12] C. Langrenne, A. Garcia, Solving of the inverse problem through a Tikhonov regularization method for an acoustic source with arbitrarily shaped surfaces, *Proceedings of Inter-Noise 1997*, 1997.
[13] S.H. Yoon, P.A. Nelson, Estimation of acoustic source strength by inverse methods: part 2, experimental investigation of methods for choosing regularization parameters, *Journal of Sound and Vibration* 233 (4) (2000) 669–705.
[14] E.G. Williams, Regularization methods for near-field acoustical holography, *Journal of the Acoustical Society of America* 110 (4) (2001) 1976–1988.
[15] Y. Kim, P.A. Nelson, Optimal regularisation for acoustic source reconstruction by inverse methods, *Journal of Sound and Vibration* 275 (2004).
[16] J. Gomes and P.C. Hansen. A study on regularization parameter choice in near-field acoustical holography. *Proceedings of Acoustics'08*, Paris, France, 2008.
[17] P.A. Nelson, S.H. Yoon, Estimation of acoustic source strength by inverse methods: part 1, conditioning of the problem, *Journal of Sound and Vibration* 233 (4) (2000) 643–668.
[18] A.P. Schuhmacher, P.C. Hansen, Sound source reconstruction using inverse bem, *Proceedings of Inter-Noise 2001*, The Hague, Holland, 2001.
[19] K.R. Holland, P.A. Nelson, Sound source characterisation: the focussed beamformer vs the inverse method, *Proceedings of ICSV 10*, Stockholm, Sweden, 2003.
[20] Q. Leclere, B. Laulagnet, An alternative acoustic imaging technique to improve capabilities of microphone array measurements, *Proceedings of NOVEM 2005*, Saint Raphael, France, 2005.
[21] M.A. Hamdi, A. Omrani, X. Ouisse, M. Mein, O. Sauvage, Presentation of a new inverse boundary element method for the determination of optimal spectral characteristics of complex noise sources, *Proceedings of Euro-Noise 2003*, Naples, Italy, 2003.
[22] M. Tournour, P. Brux, P. Mas, X. Wang, C. McCulloch, P. Vignassa, Inverse numerical acoustics of a truck engine, S.A.E. Technical Paper Series (03NVC-215), 2003.
[23] A.F. Seybert, F. Martinus, D.W. Herrin, Three experiments using the inverse bem for source identification, *Proceedings of NOVEM 2005*, Saint Raphael, France, 2005.
[24] D. Hallman, J.S. Bolton, A signal processing technique to identify the number of incoherent sources in a system, *Proceedings of Inter-Noise 92*, Toronto, Canada, July 1992, pp. 1165–1170.
[25] J.-F. Li, J.C. Pascal, C. Carles, Reconstruction of partially coherent sources by use of principal component analysis, *Proceedings of Inter-Noise 95*, Newport Beach, CA, USA, 1995.
[26] S. Dumbacher, J. Blough, D. Hallman, P. Wang, Source identification using acoustic array techniques, S.A.E. Technical Paper Series (951360), 1995.
[27] J. Verhoeven, Excitation force identification of rotating machines using operational rotor/stator amplitude data and analytical synthesized transfer functions, *Journal of Vibration, Acoustics, Stress, and Reliability in Design* 110 (1988) 307–314.
[28] P. Chevret, D. Vaucher, J.-P. Demars, R. Tilagone, Th. Colliou, B. Martin, A new generation of acoustic imaging technique for 3d sources identification: application to engine noise reduction, *Proceedings of Euronoise 2003*, 2003.
[29] G.H. Golub, M. Heath, G. Wahba, Generalized cross-validation as a method for choosing a good ridge parameter, *Technometrics* 21 (2) (1979) 215–223.
[30] P.C. Hansen, D.P. O'Leary, The use of the l-curve in the regularization of discrete ill-posed problems, *SIAM Journal on Scientific Computing* 14 (1993) 1487–1503.
[31] P.C. Hansen, *Rank-Deficient and Discrete Ill-Posed Problems*, SIAM, Philadelphia, 1998.
[32] A. Tikhonov, V. Arsenine, *Méthodes de résolution de problèmes mal posés*, Mir, Moscou, 1976.
[33] Q. Leclere, J.-L. Le Carrou, F. Gautier, Study of a concert harp's radiation using acoustic imaging methods, *Proceedings of Acoustics 08*, Paris, France, 2008.
[34] Q. Leclere, B. Laulagnet, L. Polac, Imagerie acoustique par projection en sources principales, *Proceedings of Journée SFA: Méthodes Expérimentales en Acoustique des Transports*, Guyancourt, France, 2005.
[35] L. Lamotte, Q. Leclere, Improving the localisation of sources based on shaped arrays with a reduced number of microphones, *Proceedings of Acoustics 08*, Paris, France, 2008.
[36] H.G. Choi, A.N. Thite, D.J. Thompson, Comparison of methods for parameter selection in Tikhonov regularization with application to inverse force determination, *Journal of Sound and Vibration* 304 (3–5) (2007).